Manning's Roughness Coefficient Determination in Laboratory Experiments Using 2D Modeling and Automatic Calibration

Basile Lavoie[(1)], Tew-Fik Mahdi[(2)]

[(1)] Département des génies Civil, Géologique et des Mines (CGM), École Polytechnique de Montréal, C.P. 6079, succursale Centre-Ville, Montréal, QC H3C 3A7, Canada. Email: basile.lavoie@polymtl.ca

[(2)] Professor, Département des génies Civil, Géologique et des Mines (CGM), École Polytechnique de Montréal, C.P. 6079, succursale Centre-Ville, Montréal, QC H3C 3A7, Canada (Corresponding author). Email: tewfik.mahdi@polymtl.ca

Reliable experimental data are essential for choosing and validating numerical models. Although numerous data sets have been presented in the literature, few have been made widely available to the scientific community. Additionally, these experimental data sets have generally given little attention to the determination of Manning's Roughness coefficients. This paper addresses these two issues. Three channel configurations are studied: a flatbed channel, a channel with a triangular sill and a channel with a triangular abutment. Three increasing permanent discharges are used for each configuration, leading to nine test cases. The Manning's coefficients are determined using three methods: the traditional step method, automatic calibration, via a 2D hydrodynamic model, considering theoretical value intervals and automatic calibration ignoring these intervals. The results show that automatic calibration with theoretical value intervals is advantageous compared to the step method. Automatic calibration ignoring theoretical intervals yields low errors but unphysical values; therefore, it is not recommended.

Key words:

Laboratory experiment, 2D flow modeling, PEST and SRH-2D, Automatic calibration, Triangular sill and abutment

Détermination du coefficient de rugosité de Manning dans des expériences de laboratoire utilisant la modélisation 2D et l'étalonnage automatique

Des données expérimentales fiables sont essentielles pour choisir et valider des modèles numériques. Bien que de nombreux ensembles de données aient été présentés dans la littérature, peu ont été largement diffusés auprès de la communauté scientifique. De plus, ces ensembles de données expérimentales ont généralement accordé peu d'attention à la détermination des coefficients de rugosité de Manning. Cet article aborde ces deux aspects. Des essais au laboratoire en écoulement permanent dans un canal sont réalisés. Pour ce canal, trois configurations sont étudiées: un canal à fond plat, un canal à fond plat avec un seuil triangulaire à l'aval et un canal à fond plat avec une butée triangulaire. Trois débits de valeurs croissantes sont utilisés pour chaque configuration, conduisant à neuf cas de tests. Les coefficients de Manning sont déterminés à l'aide de trois méthodes: la méthode classique des tronçons, la calibration automatique, en utilisant un modèle hydrodynamique 2D, prenant en compte les intervalles de valeurs théoriques des coefficients de Manning selon la nature des parois du canal, et la calibration automatique ignorant ces intervalles. Les résultats montrent que la calibration automatique prenant en compte les intervalles de valeurs théoriques des coefficients de Manning fournit de meilleurs résultats que la méthode des tronçons. L'étalonnage automatique ignorant les intervalles théoriques produit des erreurs faibles mais des valeurs pour les coefficients de Manning qui ne correspondent pas aux valeurs du matériau du canal; par conséquent, cette dernière méthode n'est pas recommandée. Par ailleurs, l'ensemble des données expérimentales sont fournies avec le présent article. Ces données peuvent être utilisées, sans aucune responsabilité des auteurs, sous réserve que le présent article est cité comme référence.

Mots-clefs:

Expériences de laboratoire, Modélisation 2D, PEST et SRH-2D, Calibration automatique, Seuil et butée triangulaires

I INTRODUCTION

Numerical modeling is becoming increasingly interesting for hydraulic engineers because of its speed and ease of use. Available numerical models are numerous; therefore, reliable experimental data sets are needed that allow for model validation and choice of a specific model.

This paper presents the production of a data set via the steps encountered in laboratory experimentation and data processing. Experiments in the hydraulic laboratory of the *École Polytechnique de Montréal* use three channel configurations, in which three increasing permanent discharges are studied, for a total of nine cases. The three configurations include a flatbed channel, a channel with triangular sill, and a channel with a triangular abutment.

Particular attention is paid to the determination of the Manning's roughness coefficient. Several methods have been proposed to determine this parameter (Chow 1959; French 1987; Henderson 1966):

1. The Soil Conservation Service Method, in which a basic coefficient is modified by correction factors
2. The use of theoretical tables
3. The photographic method, in which the channel is compared to other channels with known resistance values
4. Velocity measurements
5. The use of empirical formulas relating Manning's coefficient to bed material size
6. Measurement of water levels and calculation of energy slopes (step method or energy slope method)

The last method remains the most commonly used for experimentation in laboratory channels. As part of this study, this method is compared to a new method, automatic calibration, with or without regard to theoretical values. Automatic calibration is used in hydrologic and hydrodynamic studies (Ellis et al. 2009; Fabio et al. 2010; McCloskey et al. 2011; Wasantha Lal. 1995; Lin et al. 2017), but this is the first time, to the authors' knowledge, that it has been applied to retrieve Manning's roughness coefficients in a laboratory experiment with two-dimensional numerical model. The previous calibration works are mostly one-dimensional numerical models or calibrations that use few measurement points. The present study proposes to use automatic calibration with a two-dimensional model and with a very high density of water depth measurements; from 24 to 30 locations in a 6.7m x 0.762 m channel. This high density is very challenging in the search of an optimum for the automatic calibration tool and is therefore a good validation of the applicability of automatic calibration.

Moreover, the energy slope method which is usually used to determine the Manning's roughness coefficients in laboratory experiments is one-dimensional. It has been underlined (Morvan et al, 2010) that roughness coefficients may differ depending on the type of numerical model used, i.e. one-dimensional or two-dimensional models. Therefore, the use of a one-dimensional method to determine a coefficient that will be used in 2D modeling might not be the most appropriate way to proceed. Automatic calibration has the advantage of preventing that possible loss of precision.

As presented above, this article aims at two objectives:

1. Creation and distribution of a dataset to be used in validation of two-dimensional numerical models.
2. Validation of automatic calibration with 2D numerical modeling and presentation of a methodology to determine Manning's Roughness Coefficients in 2D experimental flows.

After a brief review of the available experimental data sets for numerical model validation, the paper details the experimental setup. The testing procedure is then covered, after which the various calculations necessary to identify Manning's roughness coefficients values are discussed. The results are then presented and described in order to be used as test cases to validate numerical models. Finally, concluding remarks and various recommendations are made.

II BACKGROUND

For numerical models' validation, on one hand, several researchers developed analytical solutions for simple cases. Goutal and Maurel (1997) and Delestre et al. (2013) reviewed most of these

solutions such as the ones proposed by Ritter (1892), Stoker (1957), Dressler (1954), Whitham (1955), Thacker (1981) and MacDonald et al. (1997). On the other hand, many researchers have participated in the creation and distribution of experimental data. These data sets are typically used for 1D, 2D or 3D numerical model validation. Two real data sets, the Malpasset test case (Alcrudo and Gil, 1999; Hervouet and Petitjean, 1999) and the Toce case (Valiani et al., 1999) were presented during the 4th CADAM workshop.

In recent years, considerable efforts have focused on experimental and numerical modeling of transient dam-break flows. Ozmen-Cagatay and Kocaman (2011) simulated a dam break on a horizontal bed with a trapezoidal sill and used it to compare the Reynolds-Averaged Navier Stokes and Shallow-Water equations using the CFD software Flow-3D. Similar experiments were conducted by Ozmen-Cagatay and Kocaman (2010) and LaRocque et al. (2013). Aureli et al. (2008) modeled a dam break with laboratory experiments and a finite volume code. Oertel and Bung (2012) used the observations of a dam break to validate the volume of fluid method (VOF). Soares-Frazão (2007) modeled this type of flow along a horizontal bed with a triangular sill and then against an isolated obstacle (Soares-Frazão and Zech 2007). Soares-Frazão and Zech (2008) and Testa et al. (2007) finally studied dam-break waves in idealized urban situations.

The flow around an abutment has also been given some attention. Duan (2009) studied the three-dimensional turbulent flow created around a spur dike by measuring its velocity field. Dey and Barbhuiya (2005) performed a similar experiment around a rectangular abutment.

Although all of these data sets and experiments can be effectively used to validate numerical methods and improve the understanding of the associated phenomena, careful observations raise the issue of determining Manning's roughness coefficient. Indeed, the calculation of this parameter is given relatively little attention and is never clearly explained. It is generally derived from previous experiences. This is surprising, given that it is mentioned as one of the most influential parameters in the final solutions of numerical simulations (Warmink et al. 2010). Also note that these data sets are not always made available to the scientific community; however, this issue is of great importance considering the proliferation of numerical models and the need for subsequent validation.

These two observations motivate this paper, which emphasizes calculating the Manning's roughness coefficient and providing reliable and high-quality data.

III EXPERIMENTAL SETUP

III.1 Instrumentation

Geometric levels and water depth measurements are carried out using an ultrasonic mic+340/DIU/TC sensor with an operating range of 350 to 5000 mm and an accuracy of 1% (Microsonic 2015). The flow is measured with a MAG 910E electromagnetic flowmeter, which can be applied to any conductive liquid flow (OmniInstruments 2015). The accuracy of the device is 1% for the range of flow rates used.

III.2 Channel Configurations

Three different channel configurations are used in this study. All of them were built in the Hydraulic Laboratory at École Polytechnique de Montréal. We use a rectangular flatbed channel with a steel bottom and glass walls, which is successively modified by adding a triangular sill and a triangular abutment. These modifications aim to gradually create a more complex flow. The initial geometry and the two modifications are described hereafter.

III.2.1 First Configuration – Initial Flatbed Channel

The initial channel is composed of glass walls and a steel flatbed. The zone where the flow is studied is identified in Figure 1. It has a length of 6.70 m, a width of 0.762 m and a depth of 0.764 m. Two cracks of equal dimensions are present in both channel walls at a distance of 0.882 m from the inlet boundary (figure 2), and they add a two-dimensional component to the flow. These cracks were used to support a weir in previous experiments.

The channel is relatively old; thus, the bed has been slightly modified over the years by corrosion. Therefore, a geometric survey is performed in 73 locations, improving the knowledge of the exact channel profile. Figure 3 shows these points and 24 points where the water depth was also surveyed. The blue dots represent locations where only the bed elevation is known, and red dots show locations where both the elevation and the water depth are known. These measures can be easily imported into any meshing software.

III.2.2 Second Configuration – Triangular Sill

The second studied configuration was created by adding a wooden triangular sill in the lower part of the initial channel. The sill has a length of 0.47 m and an average height of 0.126 m. Its crest is located 5.57 m downstream of the inlet boundary (Figures 4 and 5). A similar configuration was used for transient flow by Soares-Frazão (2007).

The geometrical survey used for the first configuration is upgraded by modifying 10 measurement points and adding 25 others, which brings the geometrical survey of the second configuration to a total of 98 points. There are 30 locations where the water depth is also known (Figure 6).

III.2.3 Third Configuration – Triangular Abutment

The last channel configuration is created by adding a wooden triangular abutment in the upper part of the initial channel. The abutment is symmetrical, and it has a maximum width of 0.126 m and a length of 0.48 m. Its crest is located 2.255 m from the inlet boundary (Figures 7 and 8).

The geometrical survey used for that last case is the same as the one presented for the first configuration. Only the channel boundaries need to be modified to represent the abutment. Dey and Barbhuiya (2005) showed that a vertical wall abutment induces a highly three-dimensional velocity field, which may not be well represented by a two-dimensional model such as SRH-2D which is the model used in this study and described in section *Automatic Calibration – 2D Flow – All Configurations*. Since the effect of the abutment persists downstream, the flow can be considered as locally three-dimensional and globally two-dimensional. Therefore, the 24 locations where the water depth is measured are modified and moved downstream of the abutment to capture the two-dimensional effects and avoid non-representative results in numerical modeling of 3D effects (Figure 9).

III.3 Experimental Setup

Three permanent discharges are used for each configuration presented above, leading to a total of nine different cases. These are gradually increased and will be referred to as minimum, medium and maximum discharges. The inflow is controlled through a valve and a flow sensor while the outflow is a free outfall boundary condition. To ensure steady state flow, experiments only begin after the sensor reading of the water surface elevation stabilized, which took approximately 10 minutes after opening the valve. The methodology applied for the geometric, water depth and discharge surveys are described hereafter.

III.3.1 Geometry

The geometry is measured for the three configurations in the locations previously defined in Figures 3, 6 and 9. The sensor is placed upon a sliding system (Figure 10), which is moved above the channel to obtain the levels at all determined locations. The sensor takes continuous readings and is therefore left at the same point for at least 20 seconds, allowing subsequent statistical validation and a gain in precision. The sensor gives the distance between its location and the one

where the level is needed. The level at a particular point is then given by the subtraction of that distance from the distance of the most distant point, namely, the datum. Because the sensor reacts poorly to large slopes induced by the triangular sill, the coordinates of the sill are interpolated based on the height of its crest and the level of the channel bed.

III.3.2 Water Depth

Water depths are surveyed using the same method as that used for the geometry. The water depth is computed by subtracting the distance from the sensor to the water surface and the distance from the sensor to the channel bed.

III.3.3 Discharge

The discharge entering the channel is controlled with a valve and measured by a flow sensor. Because the water depth is not measured simultaneously, an experiment can last up to an hour; therefore, the discharge may show small variations over the duration of the experiment. To verify these variations, discharges are recorded every three minutes and statistically validated after the experiment.

IV STATISTICAL TREATMENT

As previously mentioned, every value is represented by a series of measurements of the same phenomenon. A statistical treatment is therefore applied to these series to determine the single value that best represents reality. Protassov (2002) proposed that an experimental value resulting from a finite number of measurements may be expressed via equations 1 and 2:

$$l_{exp} \pm \Delta l = m \pm s_m t_{vP} \tag{1}$$

$$s_m = \frac{1}{N(N-1)} \sum_{I=1}^{N} (l_i - m)^2 \tag{2}$$

where l_{exp} is the experimental average value; Δl is its uncertainty; m and s_m are the average and standard deviation, respectively, of a series of measured values; t_{vP} is the Student Coefficient; N is the number of measurements; and l_i is a measured value.

The following method is applied to the three types of measurements (discharge, water depth and geometry):

1. Computation of the experimental average value (l_{exp}=m), experimental standard deviation (s_m), number of freedom degrees and Student coefficient (t_{VP});
2. Calculation of uncertainty (Δl).

Changing the datum for every geometry level and water depths requires subtraction, and the sum of the uncertainty is then used as the final uncertainty. The x- and y-coordinates are measured with a measuring tape that is fixed on the edge of the channel and marked to ensure that the sensor can always be moved and positioned at exact desired locations. Half of the smallest measurement level of the tape is used as the uncertainty. Table 1 shows that the uncertainties are relatively small, with the highest associated with the x- and y-coordinates. The inflows to which they refer are detailed in the *Presentation of Data Sets* section, while the water depths and coordinates are given in appended text files.

Experimental repeatability is verified in the channel with an abutment (third configuration), and all the manipulations and statistical treatments are repeated twice at the medium discharge level. Measurements are made when the flow-meter indicates a steady discharge at the inlet. Once the first set of measurements is done, the channel is totally emptied and the process can be repeated. When compared, the two experiments present very small differences for both the discharge (RMSE=0.000678 m^3/s) and water depth (RMSE=0.00022 m, maximum residual=0.00198).

V DETERMINATION OF MANNING'S ROUGHNESS COEFFICIENTS

Manning's roughness coefficient is calculated in three different ways: the one-dimensional step method (Chow, 1959 and Henderson 1966), automatic calibration considering the theoretical Manning's value intervals of the channel materials (2D) and automatic calibration ignoring the theoretical Manning's value intervals of the channel materials (2D). The step method is applied to the flatbed channel (first configuration) only, and the automatic calibrations are performed for all three configurations. These methods all consider the minimum discharge. The Manning's roughness coefficient is then used for medium and maximum discharges. Since the roughness coefficient varies with the wetted perimeter, there might be a difference between coefficients for the minimum, medium and maximum discharges and their respective water depths. To use a single coefficient for all three discharges, we do the hypothesis that with the present configuration, the coefficient variations are small enough to be neglected. The validity of this hypothesis is verified in the *Automatic Calibration with Respect to Theoretical Intervals* section where the Manning's coefficient provided by the calibration for minimum and maximum discharges are found to be very similar.

V.1 Instrumentation

Manning's coefficient is considered uniform throughout the whole domain of the initial flatbed channel and the channel with the triangular abutment (configurations 1 and 3), while it is composed of two materials for the channel with a wooden triangular sill (configuration 2). These materials are represented based on the Manning's coefficient intervals proposed by Chow (1959) for corrugated metal, wood and glass. Because the main part of the channel is composed of a steel bed with glass walls, the coefficient intervals are computed from the equivalent Manning's constant equation (Chaudhry 2008). These intervals are computed for the channel with the triangular sill at a distance of 1.1 m from the inlet boundary and are also used for the two other configurations. The water depth varies considerably over the sill (hmin=hc=0.017 m and hmax=0.20 m), but it occurs over a very short distance (0.47 m). Therefore, no equivalent Manning's coefficient is computed for that location. The Manning's coefficient equation is as follows:

$$n_c = \frac{\left[\sum P_i n_i^{3/2}\right]^{2/3}}{P^{2/3}} \tag{3}$$

where n_c and P are the equivalent Manning's roughness coefficient and wetted perimeter of the whole section, respectively, while n_i and P_i are for a subsection associated with a specific material.

In the step method, calibration values are verified with the theoretical intervals created by the maximum and minimum values presented in Table 2. For automatic calibration, these intervals are used as limiting values.

V.2 Step Method – 1D Flow – Flatbed Channel

This method is only used for the flatbed channel (first configuration) at the minimum discharge. The Manning's coefficient for the equivalent sections made of steel and glass is first computed with the step method (Henderson 1966):

$$\Delta x = \frac{\Delta E}{J_f - J_e} \tag{4}$$

$$J_e = \frac{V^2 n^2}{R_h^{4/3}} \tag{5}$$

where Δx is the spatial variation in the x-direction, ΔE is the energy variation, J_f is the bed slope, J_e is the energy slope and R_h is the hydraulic radius.

We use the minimum discharge in the initial flatbed channel, for which the Manning's coefficient is calculated in every section bound by two measured water depths. The hydraulic radius is calculated from averaged value of the water depth over a cross-section. When calculated using the step method, the Manning's roughness coefficients range from 0.012 to 0.017, with an average value of 0.014.

Figure 11 presents the difference observed between Manning's roughness coefficient calculated with the step method and that recommended by the theory. The calculated coefficients are slightly below the theoretical values. This may be explained by the fact that these coefficients were determined for one-dimensional flow which is not completely achieved with the flatbed configuration. Also theoretical intervals where determined for materials that are not identical to those used in this study, such variations are therefore reasonable.

V.3 Automatic Calibration – 2D Flow – All Configurations

Automatic calibration is used to retrieve Manning's roughness coefficients for the three channel configurations at the minimum discharge. Three models are used in this paper, including the finite-volume code SRH-2D (Lai 2008), the pre-treatment and post-treatment software SMS (AQUAVEO 2016) and the automatic calibration model PEST (Doherty 2005).

V.3.1 SRH-2D

SRH-2D solves the shallow-water equations of the following form (Lai 2008).

$$\frac{\partial h}{\partial t}+\frac{\partial hU}{\partial x}+\frac{\partial hV}{\partial x}=e \tag{6}$$

$$\frac{\partial hU}{\partial t}+\frac{\partial hUU}{\partial x}+\frac{\partial hVU}{\partial y}=\frac{\partial hT_{xx}}{\partial x}+\frac{\partial hT_{xy}}{\partial y}-gh\frac{\partial z}{\partial x}-\frac{\tau_{bx}}{\rho} \tag{7}$$

$$\frac{\partial hV}{\partial t}+\frac{\partial hUV}{\partial x}+\frac{\partial hVV}{\partial y}=\frac{\partial hT_{xy}}{\partial x}+\frac{\partial hT_{yy}}{\partial y}-gh\frac{\partial z}{\partial y}-\frac{\tau_{by}}{\rho} \tag{8}$$

The friction is determined using the Manning equation:

$$\begin{pmatrix}\tau_{bx}\\ \tau_{by}\end{pmatrix}=\rho C_f\begin{pmatrix}U\\ V\end{pmatrix}\sqrt{U^2+V^2} \tag{9}$$

$$C_f=\frac{gn^2}{h^{\frac{1}{3}}} \tag{10}$$

Boussinesq equations are used to compute the turbulent stresses:

$$T_{xx}=2(\nu+\nu_t)\frac{\partial U}{\partial x}-\frac{2}{3}k \tag{11}$$

$$T_{xy}=(\nu+\nu_t)\left(\frac{\partial U}{\partial y}-\frac{\partial V}{\partial x}\right) \tag{12}$$

$$T_{yy}=2(\nu+\nu_t)\frac{\partial V}{\partial y}-\frac{2}{3}k \tag{13}$$

where h is the water depth, u and v are the velocity components, e is a source term, T is the turbulent stress, τ is the shear stress, g is the gravitational acceleration, ρ is the mass density, μ_0 is the kinematic viscosity of water, μ_t is the turbulent eddy viscosity and k is the turbulent kinetic energy.

SRH-2D proposes two turbulence models: the k-epsilon and depth-averaged parabolic models. The k-epsilon model with default parameters values is used in this article.

V.3.2 SMS

The Surface-water Modeling System (SMS; (AQUAVEO 2016) allows the user to execute the required pre-treatment and post-treatment procedures for hydraulic modeling of open channel flow. The pre-treatment includes the importation of geometry points, definition of the digital elevation model, interpolation of elevations via triangulation and creation of mesh. The post-treatment capabilities include the visualization of results in three-dimensions.

V.3.3 PEST

PEST (Doherty 2005) is a software that performs automatic calibration and sensitivity analysis of any model based on input and output files in binary or text formats. Only the automatic calibration module is used in this paper. For the present application, the user first has to set up a normal simulation with values of elevations, materials and boundary conditions and ensure that this simulation runs properly. PEST is then used to do and control several runs of the simulation while varying the calibrated parameter (roughness coefficient) and comparing the results with observation data (provided by the modeler). At the end of this process, a calibrated parameter that lower the difference between modeled and observed values of water depth is determined. Automatic calibration with PEST requires three main types of file: template, instruction and control files. The template files act as models for PEST when creating input files to calibrate the model (SRH-2D). Instruction files aid PEST in the interpretation of the model's output by indicating the values that should be used in the calibration. The control file contains calibration instructions, such as stopping criteria, and observed values. It relates the template and instruction files to the associated model files. The process is detailed in figure 12.

V.3.4 Flow Modeling

The meshes are composed of triangular elements with an average side size of 0.05 m. Based on the channel, meshes have lengths of 6.7 m and widths of 0.762 m. Boundary conditions are applied as defined in the *Presentation of Data Sets section* and the minimum discharge is used. The experimental setup presents a channel with a free outfall boundary conditions and therefore a critical depth. However, the critical depth before a freefall is hard to locate precisely and this would create some uncertainties for numerical modeling. Instead, the last row of measurements (x=6.7 m) is averaged to give a mean depth that is utilized as a numerical boundary condition. The total simulation time is 15 minutes, ensuring that the model reaches a steady flow conditions and that flow depths do not vary in time, i.e. the water depth do not vary between the two last time step. A sensitivity analysis has been done previously to determine a time step that ensure a balance between numerical stability, quality of results and computation time. A time step of 0.1 seconds was found to be adequate. Figure 13 shows the three meshes used to model and calibrate the three configurations.

V.3.5 Automatic Calibration with Respect to Theoretical Intervals

Automatic calibration is then performed using theoretical intervals. This method aims to determine Manning's coefficients that minimize the difference between observed and modeled water depths, while maintaining values that are physically representative of the real channel. This method is used for all three channels at the minimum discharge rate. Additionally, all the measured water depths, except the outflow boundary conditions, are used in the calibration, specifically, 21 locations in the flatbed channel and the channel with the abutment and 27 locations in the channel with the triangular sill. When computed in this manner, the coefficients lead to an RMSE that is

relatively small for configurations 1 and 3 and a bit higher for configuration 2, likely because the presence of a second material complicates the search for an optimum (Table 3).

As stated in section *Determination of Manning's Roughness Coefficients,* the hypothesis was made that a coefficient calibrated with the minimum discharge could be used with the medium and maximum discharges. To verify this, automatic calibration of the flatbed channel is also performed with the maximum discharge and calibrated coefficients for minimum and maximum discharges are compared. The roughness coefficient determined for the steel/glass compound section and the maximum discharge is 0.0176 $s/m^{1/3}$. This is very close to the value obtained for the minimum discharge ($0.017 s/m^{1/3}$). These results support the use of same Manning's coefficients with all discharges in the present test-cases.

V.3.6 Automatic Calibration Ignoring Theoretical Intervals

To evaluate the impacts of the chosen intervals on the results of the PEST calibration, a second series of calibrations is performed with larger intervals of 0.005 to 0.05 that do not account for the theoretical values. The Manning's roughness coefficients computed for the flatbed channel and channel with the triangular abutment are similar to those calculated previously, and their RMSEs are less than half of the previous values (Table 4). However, the coefficients calculated for the channel with the triangular sill are very different but have similar RMSEs. Additionally, these coefficients are inconsistent with the theoretical results because they yield larger roughness values for the wood, which is contradicted by visual inspection. These results emphasize the importance of carefully defining the calibration intervals to prevent the model from converging to a non-physical optimum.

V.4 Comparison of Calibration Methods

Figure 14 compares the errors calculated based on the water depths in the flatbed channel when modeled with SRH-2D via SMS, with Manning's coefficients computed by the three aforementioned methods. The step method gives the most important RMSE, followed by automatic calibration with consideration of theoretical intervals. Both are superior to the automatic calibration that ignores theoretical intervals. However, considering the non-physical values resulting from that method for the channel with the triangular sill, the automatic calibration with chosen intervals remains the best method. The fact that automatic calibration with theoretical intervals provides a smaller RMSE than the step method for the simplest configuration studied, even with a small difference, supports the ability of this method to retrieve Manning's roughness coefficients. Therefore, this method becomes particularly applicable for experimental setups where more than one material is used or setups with two-dimensional flow that are not properly represented by the step method. The possibility of coupling PEST with any model offers the flexibility to find the Manning's coefficient of a certain type of flow with the most appropriate model according to the user's judgement.

VI PRESENTATION OF DATA SETS

Table 5 presents a summary of the available data sets for the three channel configurations. For each configuration, three discharges are available, with corresponding boundary conditions.

The boundary conditions include discharge at the inflow boundary and a water depth at the outflow boundary. The water depth is an average of three measured water depths at the outflow boundary, specifically, 6.7 m from the inlet. Table 6 shows the final Manning's roughness coefficients that should be used by the modeler.

The results are available in three supplementary data files (*Configuration_1.pdf*, *Configuration_2.pdf*, *Configuration_3.pdf*). The three files contain three series of water depths, one for each discharge. All coordinates and water depth values are in SI units.

VII CONCLUSION

This paper presents the acquisition and processing of the geometric and water depth data in nine flow cases, including three discharges in three channel configurations. These data sets were statistically processed, and the Manning's coefficients were determined by three different methods: calculating the energy slope, automatic calibration taking into account the theoretical coefficient intervals and automatic calibration ignoring these intervals. These three methods are compared, and it appears that automatic calibration is advantageous if it takes into account the theoretical intervals; otherwise, the model may converge to a global optimum that is not physically representative of the situation. The acquired data sets are given in appended text files, and the SMS and SRH-2D files used are available upon request. Users are invited to use these data sets in their studies with proper citation of the source.

VIII NOMENCLATURE

e	Source term;
g	Gravitational acceleration;
h	Water depth;
J_e	Energy slope;
J_f	Bed slope;
k	Turbulent kinetic energy;
l_{exp}	Experimental value ("ell");
l_i	Measured value ("ell");
m	Average measured value;
N	Number of measurements;
n	Manning's roughness coefficient;
n_c	Equivalent Manning's roughness coefficient;
n_i	Manning's roughness coefficient of a subsection;
P	Wetted perimeter;
R_h	Hydraulic radius;
s_m	Standard deviation of a series of measured values;
T	Turbulence stress;
t	Time;
t_{vP}	Student coefficient associated with a degree of freedom and probability;
u	Velocity component (x-direction);
v	Velocity component (y-component);
ΔE	Energy variation;
Δl	Uncertainty of an experimental value;
Δx	Spatial variation in the x-direction;
μ_0	Kinematic viscosity of water;
μ_t	Turbulent eddy viscosity;
ρ	Mass density;
τ	Shear stress.

IX ACKNOWLEGMENTS AND THANKS

This research was supported in part by a National Science and Engineering Research Council (NSERC) Discovery Grant, application No: RGPIN-2016-06413.

X REFERENCES

Alcrudo, F. and Gil, E. (1999). The Malpasset dam break case study the 4th CADAM Workshop, Zaragoza, 95-109.

AQUAVEO (2016). "SMS 12.1 - The Complete Surface-water Solution." <http://www.aquaveo.com/software/sms-surface-water-modeling-system-introduction>. (March 10, 2016).

Aureli, F., Maranzoni, A., Mignosa, P., and Ziveri, C. (2008). "Dam-Break Flows: Acquisition of Experimental Data through an Imaging Technique and 2D Numerical Modeling." *Journal of Hydraulic Engineering*, 10.1061/(ASCE)0733-9429(2008)134:8(1089), 1089-1101.

Chaudhry, H. (2008). *Open-Channel Flow*, Springer Science, New-York.

Chow, V. T. (1959). *Open-Channel Hydraulics*, McGraw-Hill, New-York.

Delestre, O., Lucas, C., Ksinant, P.-A., Darboux, F., Laguerre, C., Vo, T. N. T., James, F., and Cordier, S. (2013). SWASHES: a compilation of Shallow-Water analytic solutions for hydraulic and environmental studies. International Journal for Numerical Methods in Fluids, 72:269–300.

Dey, S., and Barbhuiya, K. (2005). "Flow Field at a Vertical-Wall Abutment." *Journal of Hydraulic Engineering*, 10.1061/(ASCE)0733-9429(2005)131:12(1126), 1126-1135.

Dressler, R. F. (1954). Comparison of theories and experiments for the hydraulic dam-break wave. *International Association of Sciences Hydrology*, **3** (38), 319–328.

Doherty (2005). "PEST, Model-Independant Parameter Estimation, USer Manual: 5th Edition." Watermark Numerical Computing.

Duan, J. G. (2009). "Mean Flow and Turbulence around a laboratory Spur Dike." *Journal of Hydraulic Engineering*, 10.1061/(ASCE)HY.1943-7900.0000077, 803-811.

Ellis, R. J. l., Doherty, J., Searle, R. D., and Moodie, K. (2009). "Applying PEST (Parameter ESTimation) to improve parameter estimation and uncertainty analysis in WaterCAST models." *18th World IMACS/MODSIM Congress*, Modelling and Simulation Society of Australia and New-Zealand Inc., 3158-3164.

Fabio, P., Aronica, G. T., and Apel, H. (2010). "Towards automatic calibration of 2-D flood propagation models." *Hydrology and Earth System Sciences*, 10.5194/hess-14-911-2010, 911-924.

French, R. H. (1987). *Open Channel Hydraulics*, McGraw-Hill Book Company, New-York.

Goutal, N. and Maurel, F. (1997). Proceedings of the 2nd workshop on dambreak wave simulation. Technical Report HE-43/97/016/B, Electricité de France, Direction des études et recherches.

Henderson, F. M. (1966). *Open Channel Flow*, Macmillan Publishing Co., Inc., New-York.

Hervouet, J. M. and Petitjean, A. (1999). Malpasset dam-break revisited with two-dimensional computations Journal of Hydraulic Research, 37(6), 777-788.

Lai, Y. G. (2008). "SRH-2D version 2: Theory and User's Manual." U.S. Department of the interior - Bureau of Reclamation, Denver.

LaRocque, L. A., Imran, J., and Chaudhry, M. H. (2013). "Experimental and Numerical Investigations of Two-Dimensional Dam-Break Flows." *Journal of Hydraulic Engineering*, 10.1061/(ASCE)HY.1943-7900.0000705, 569-579.

Lavoie, B. and Mahdi, T. (2016). “Comparison of two-dimensional Flood Propagation Models: SRH-2D and HYDRO_AS-2D.” *Natural Hazards,*10.1007/s11069-016-2737-7, 1207-1222

Lin, F.-R., Wu, N.-J., Tu, C.-H., Tsay, T.-K. (2017). “Automatic Calibration of an Unsteady River Flow Model by Using Dynamically Dimensioned Search Algorithm.” *Mathematical Problems in Engineering,*10.1155/2017/7919324, 19 pages

MacDonald, I., Baines, M. J., Nichols, N. K. and Samuels, P. G. (1997). Analytic benchmark solutions for open-channel flows Journal of Hydraulic Engineering. 123(11), 1041-1045

McCloskey, G. L. l. E., R.J., Waters, D. K., and Stewart, J. (2011). "PEST hydrology calibration process for source catchments - applied to the Great Barrier Reef, Quennsland." *19th International Congress on Modelling and Simulation*, Modelling and Simulation Society of Australia and New-Zealand Inc., 2359-2366.

Microsonic (2015). "mic+340/IU/TC." <http://www.microsonic.de/en/distance-sensors/cylindrical/micplus/standard-sensors/standard-sensors/micplus340iutc.htm>. (March, 12, 2016).

Morvan, H., Knight, D., Wright, N., Tang, XN and Crossley, A. (2010). "The concept of roughness in fluvial hydraulics and its formulation in 1D, 2D and 3D numerical simulation models" *Journal of Hydraulic Research,* 10,1080/00221686.2008.9521855, 191-208.

Oertel, M., and Bung, D. (2012). "Initial stage of two-dimensional dam-break waves: laboratory versus VOF." *Journal of Hydraulic Research*, 10.1080/00221686.2011.639981, 89-97.

OmniInstruments (2015). "MAG 910 Electromagnetic Flowmeter." <http://www.omniinstruments.co.uk/flow-meters/electromagnetic-flow-meters-magnetic-flow-meters/mag910e-magnetic-flowmeter.html>. (March, 12, 2016).

Ozmen-Cagatay, H., and Kocaman, S. (2010). "Dam break flows during initial stage using SWE and RANS approaches." *Journal of Hydraulic Research*, 10.1080/00221686.2010.507342, 603-611.

Ozmen-Cagatay, H., and Kocaman, S. (2011). "Dam-Break Flow in the Presence of Obstacle: Experiment and CFD Simulation." *Engineering Applications of Computational Fluid Mechanics*, 10.1080/19942060.2011.11015393, 541-552.

Protassov, K. (2002). *Analyse statistique de données expérimentales*, EDP Sciences, Les Ulis.

Ritter, A. (1892). Die Fortpflanzung der Wasserwellen. Vereine Deutcher Ingenieure Zeitswchrift, 36, 947-954.

Soares-Frazão, S. (2007). "Experiments of dam-break wave over a triangular bottom sill." *Journal of Hydraulic Research*, 10.1080/00221686.2007.9521829, 19-26.

Soares-Frazão, S., and Zech, Y. (2007). "Experimental study of dam-break flow against an isolated obstacle." *Journal of Hydraulic Research*, 10.1080/00221686.2007.9521830, 27-36.

Soares-Frazão, S., and Zech, Y. (2008). "Dam-break flow through an idealised city." *Journal of Hydraulic Research*, 10.3826/jhr.2008.3164, 648-658.

Stoker, J. J. (1957). Water Waves: The Mathematical Theory with Applications Interscience Publishers, New York, USA.

Testa, G., Zuccalà, D., Alcrudo, F., Mulet, J., and Soares-Frazão, S. (2007). "Flash flood flow experiment in a simplified urban district." *Journal of Hydraulic Research*, 10.1080/00221686.2007.9521831, 37-44.

Thacker, W. C. (1981). Some exact solutions to the nonlinear shallow-water wave equations. Journal of Fluid Mechanics Digital Archive, 107, 499-508

Valiani, A., Caleffi, V. and Zanni, A. (1999). Finite Volume scheme for 2D Shallow-Water equations: Application to a flood event in the Toce river the 4th CADAM Workshop, Zaragoza, 185-206.

Warmink, J. J., Van der Klis, H., Booij, M. J., and Hulscher, S. J. M. H. (2010). "Identification and Quantification of Uncertainties in a Hydrodynamic River Model Using Expert Opinions." *Water Resources Management*, 10.1007/s11269-010-9716-7, 601-622.

Wasantha Lal, A.M. (1995). "Calibration of Riverbed Roughness."*Journal of Hydraulic Engineering"*, 10.1061/(ASCE)0733-9429(1995)121:9(664)*, 664-671.*

Whitham, G. (1955). The effects of hydraulic resistance in the dam-break problem. Proc. Roy. Soc. of London, Ser. A., 227, 399-407

XI TABLES

Table 1. Uncertainties in measured values

Measured value	Maximum uncertainty
Water depth (m)	3.65×10^{-4}
Discharge (m^3/s)	3×10^{-3}
X-coordinate (m)	1×10^{-3}
Y-coordinate (m)	1×10^{-3}
Z-coordinate (m)	1.3×10^{-4}

543

Table 2. Theoretical intervals of Manning's roughness coefficient

Material	Minimum value ($s/m^{1/3}$)	Maximum value ($s/m^{1/3}$)
Corrugated metal[a]	0.021	0.030
Wood[a]	0.010	0.014
Glass[a]	0.009	0.013
Equivalent constant Manning – steel/glass	0.017	0.028

[a]Based on Chow (1959)

544

545

Table 3. Manning's coefficients determined with automatic calibration for theoretical intervals

Configuration	Manning's Coefficient ($s/m^{1/3}$)		Error (m)	
	Steel/Glass	Wood	RMSE	Max. Residual
Flatbed channel	0.0170	-	0.0019	0.0032
Channel with sill	0.0174	0.0140	0.0116	0.0215
Channel with abutment	0.0170	-	0.0022	0.0044

Table 4. Manning's coefficients determined with automatic calibration ignoring theoretical intervals

	Manning's Coefficient ($s/m^{1/3}$)		Error (m)	
	Steel/Glass	Wood	RMSE	Max. Residual
Flatbed channel	0.0155	-	0.0007	0.0018
Channel with sill	0.0050	0.05	0.0097	0.0187
Channel with abutment	0.0151	-	0.001	0.0022

Table 5. Boundary conditions

Boundary Conditions	Minimum Inflow		Medium Inflow		Maximum Inflow	
	Inlet BC (m^3/s)	Outlet BC (m)	Inlet BC (m^3/s)	Outlet BC (m)	Inlet BC (m^3/s)	Outlet BC (m)
Flatbed channel	0.031	0.074	0.073	0.120	0.101	0.144
Channel with sill	0.041	0.035	0.070	0.055	0.108	0.078
Channel with abutment	0.040	0.086	0.064	0.112	0.100	0.140

Table 6. Final Manning's roughness coefficients

Material	Manning's roughness coefficient ($s/m^{1/3}$)
Steel/Glass	0.017
Wood (sill)	0.014

546

547

FIGURE CAPTIONS

Fig. 1 Initial flatbed channel

Fig. 2 Crack geometry

Fig. 3 First configuration - Positions of geometric and water depth surveys

Fig. 4 Second configuration – Flow over a triangular sill

Fig. 5 Second configuration - Sectional view

Fig. 6 Second configuration - Positions of geometric and water depth surveys

Fig. 7 Third configuration – Flow around a triangular abutment

Fig. 8 Third configuration – Plan view

Fig. 9 Third configuration - Positions of geometric and water depth surveys

Fig. 10 Sensor on the sliding system

Fig. 11 Comparison of the theoretical and step methods for calculating Manning's coefficients in the initial flatbed channel

Fig. 12 Automatic calibration with PEST – From Lavoie and Mahdi (2016)

Fig. 13a Mesh of the initial flatbed channel

Fig. 13b Mesh of the channel with the triangular sill

Fig. 13c Mesh of the channel with the triangular abutment

Fig. 14 Comparison of water depth RMSEs calculated using SRH-2D for the three calibration methods

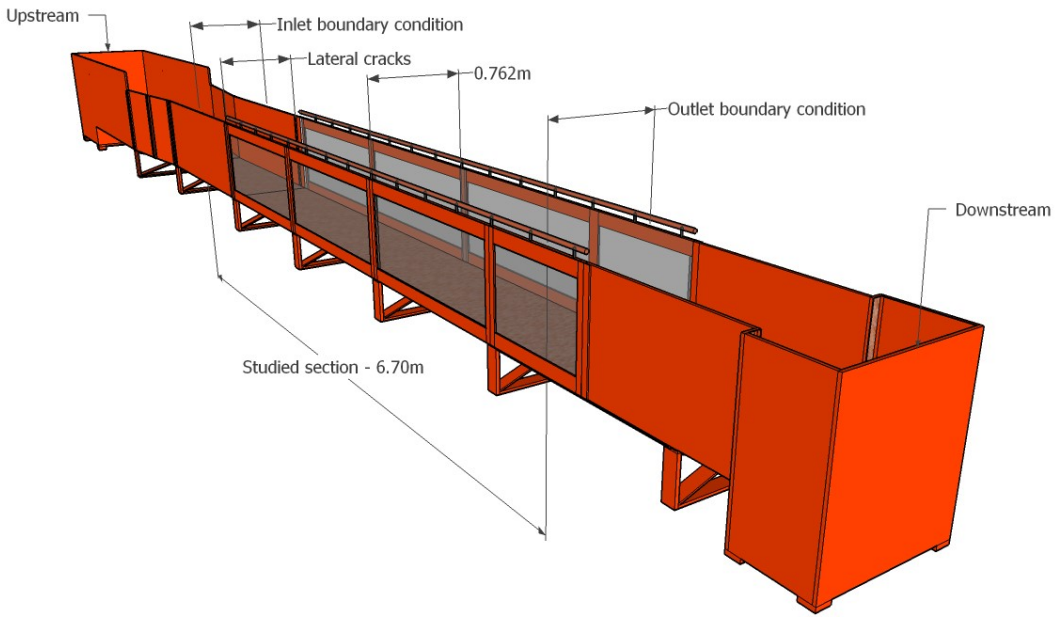

568

569 Fig.1

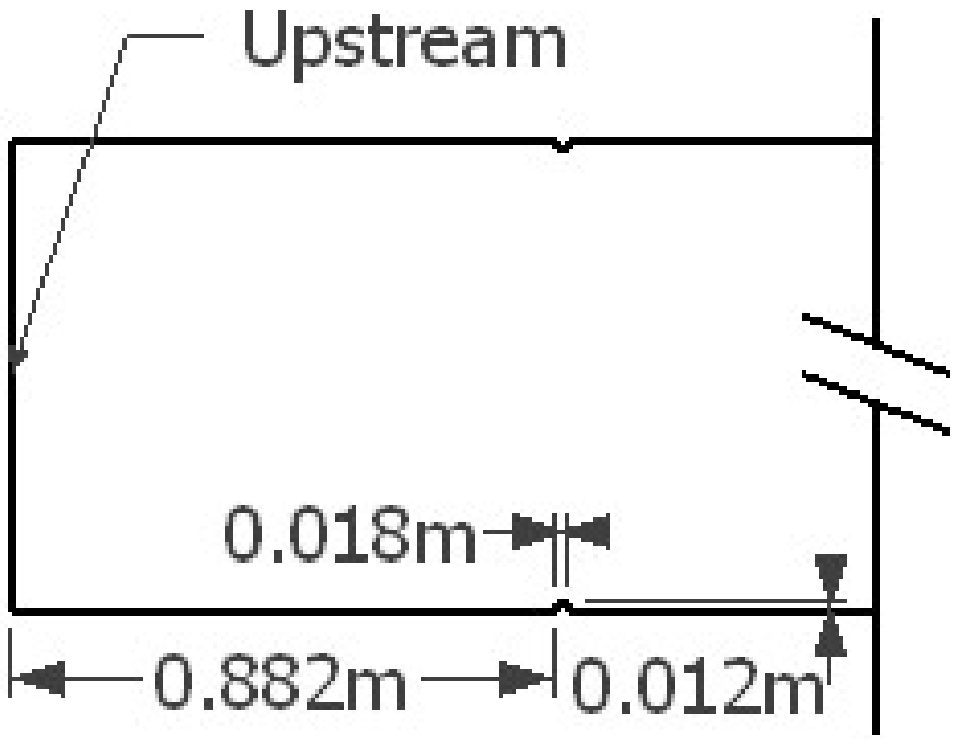

570 Fig.2

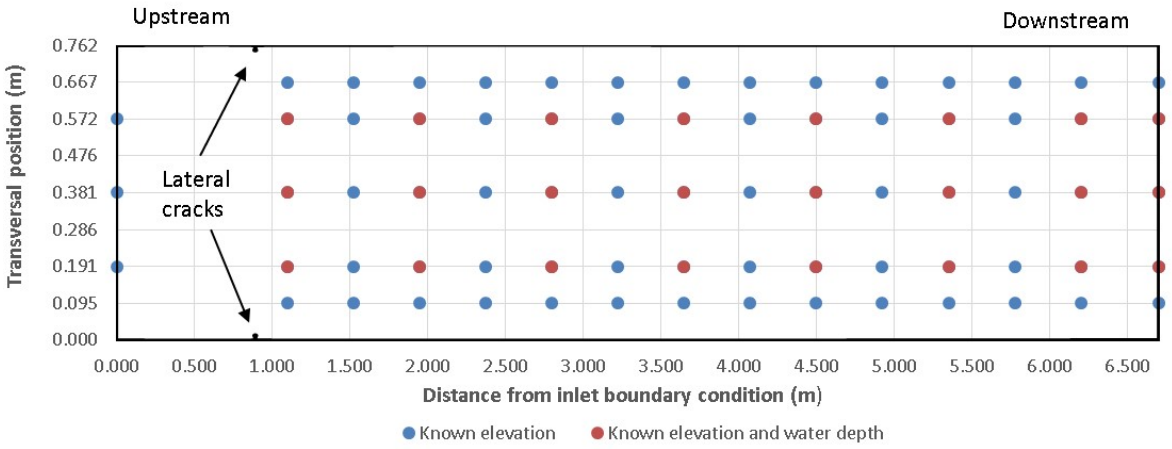

571

572 Fig. 3

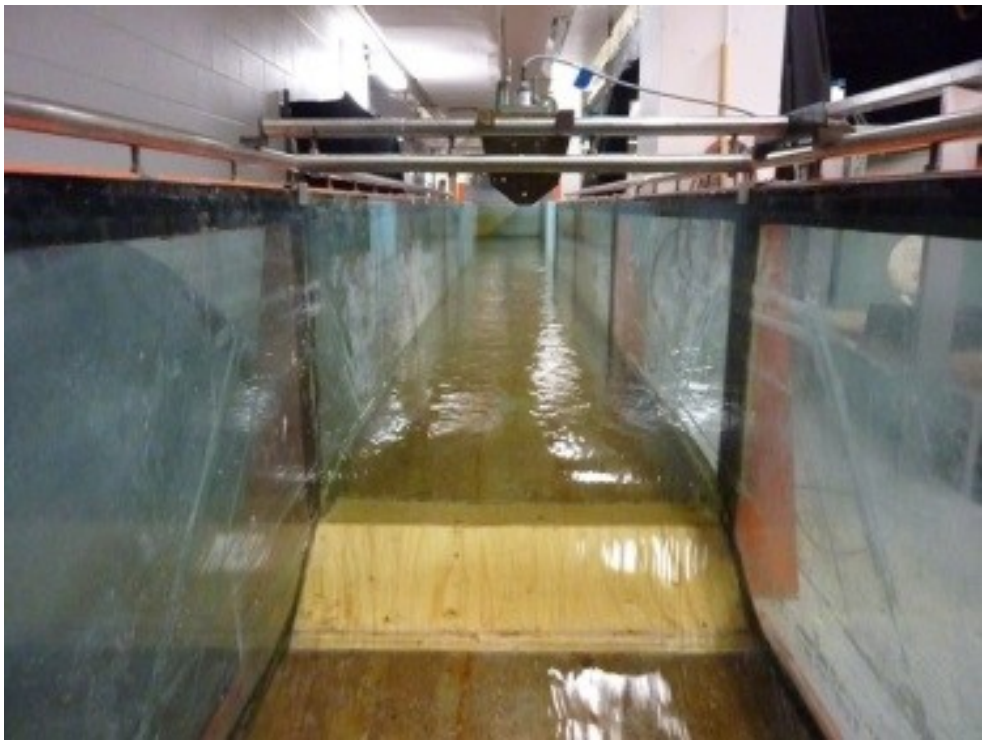

573

574 Fig. 4

575

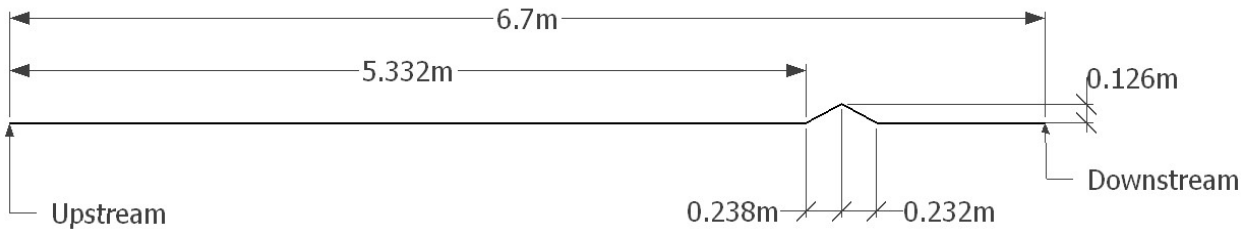

576

577 Fig. 5

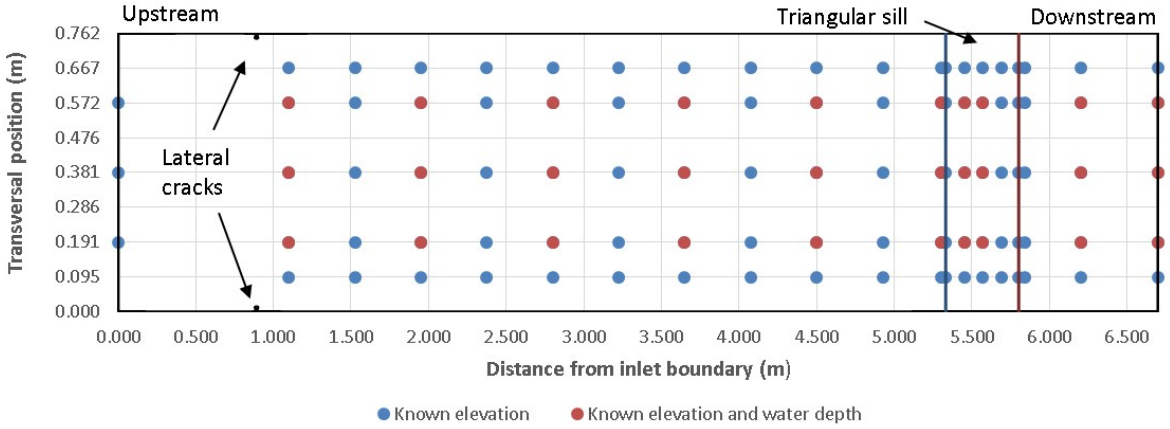

578

579 Fig. 6

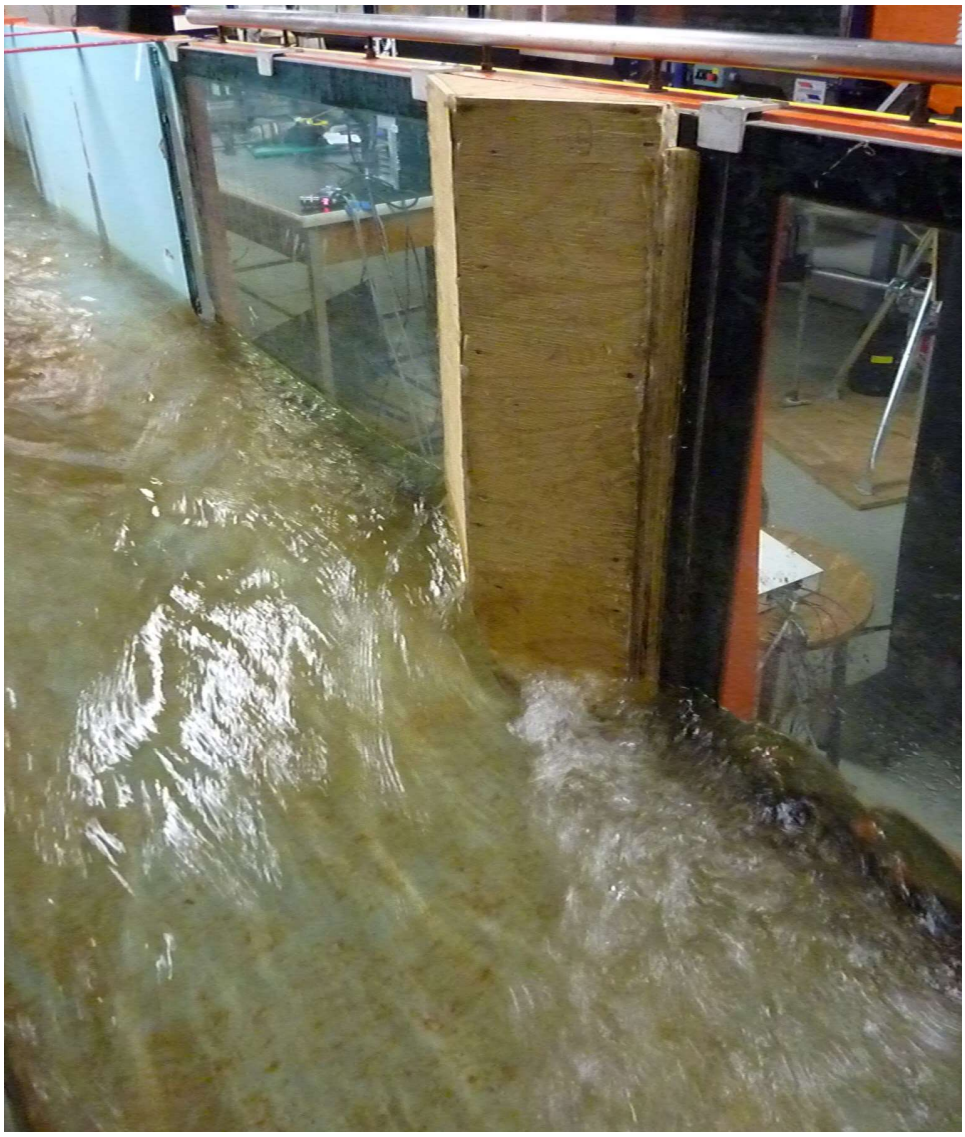

580

581 Fig. 7

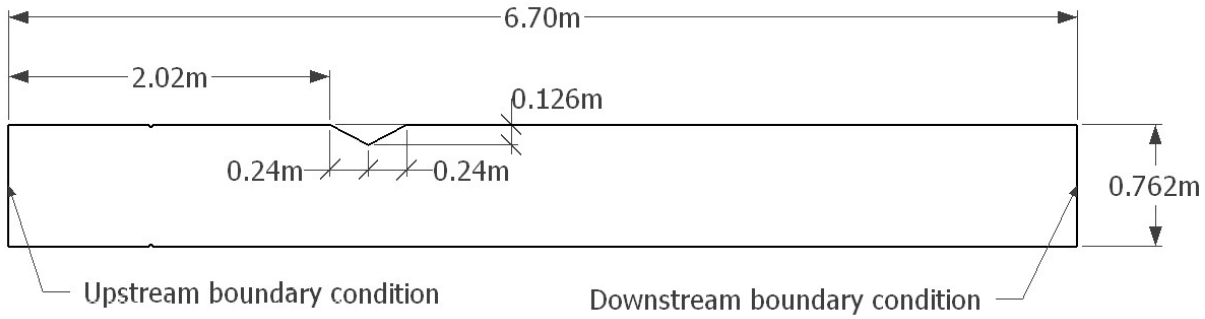

582

583 Fig. 8

584

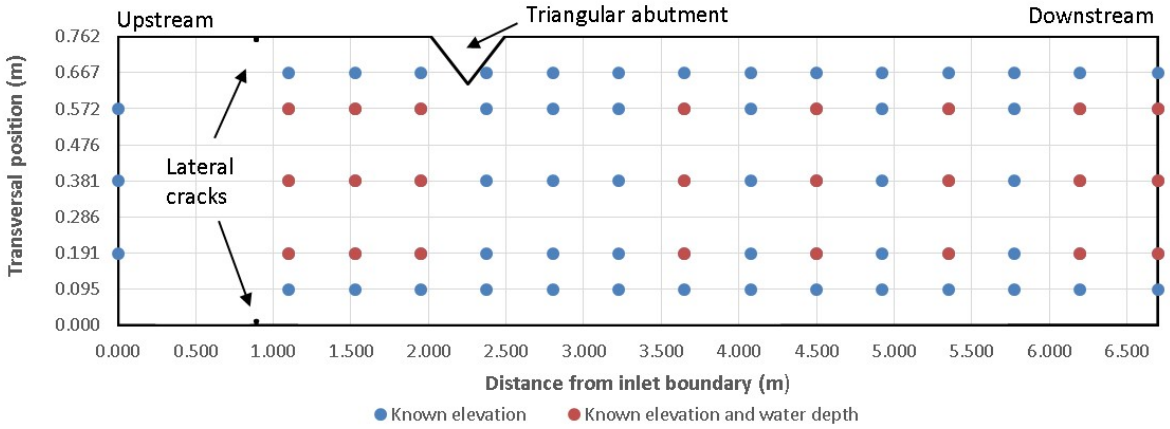

585

586 Fig. 9

587

588

589 Fig. 10

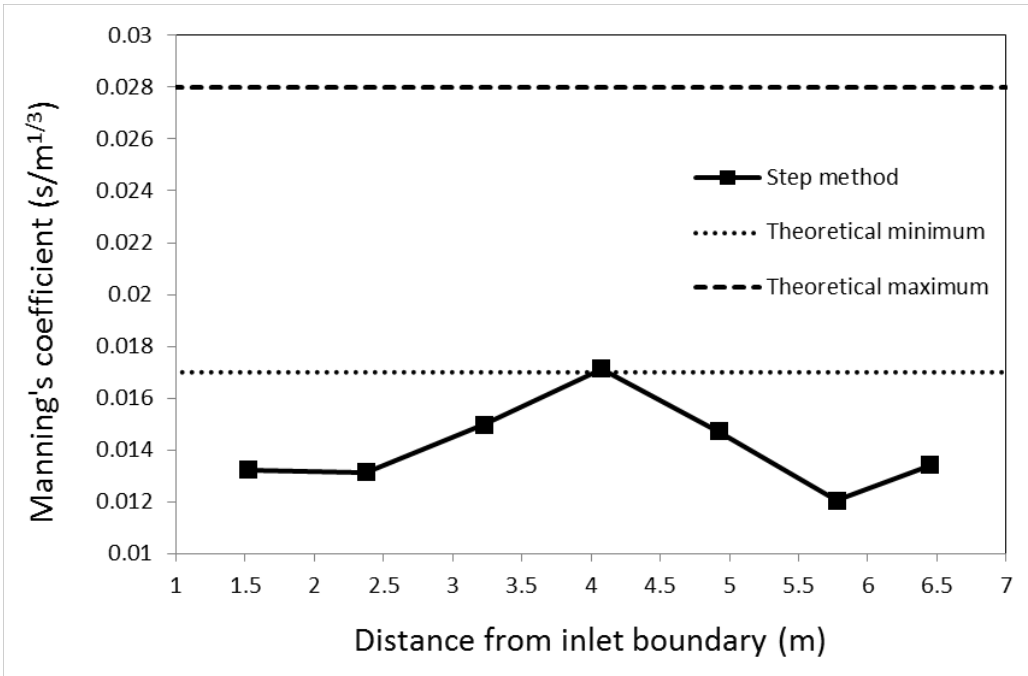

590

591 Fig. 11

592

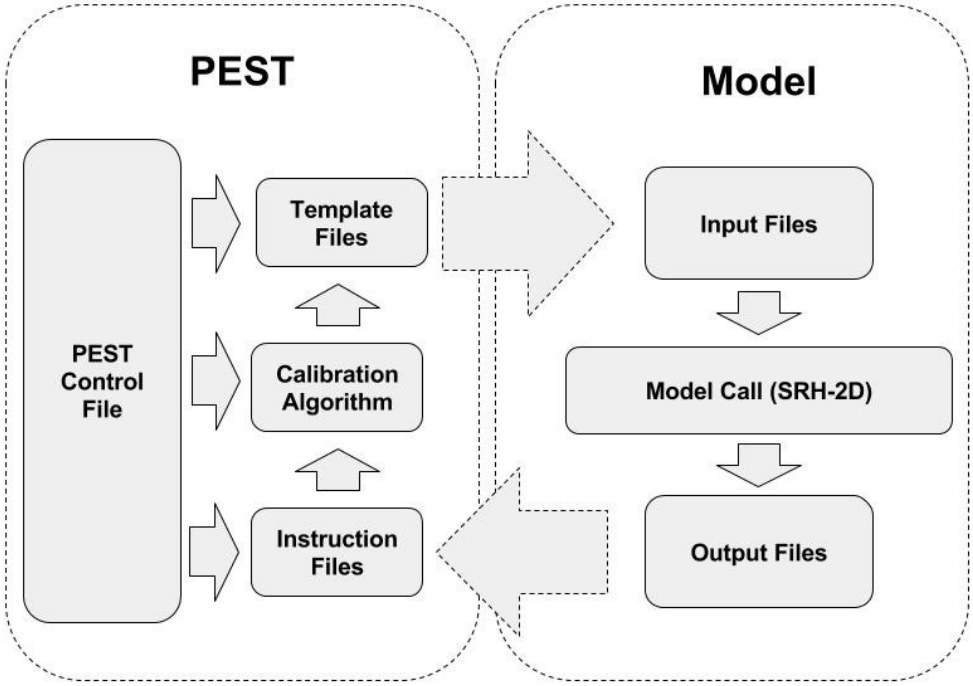

593

594 Fig. 12

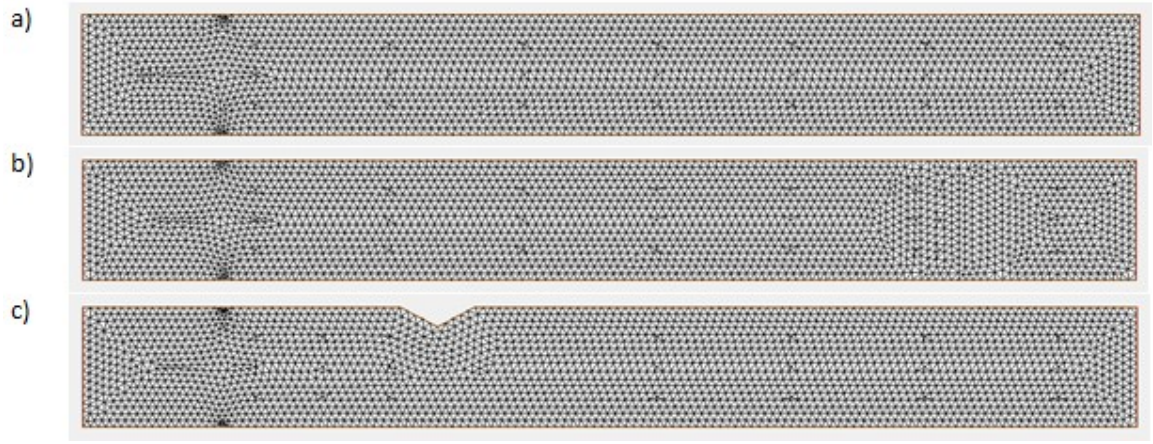

595

596 Fig. 13

597

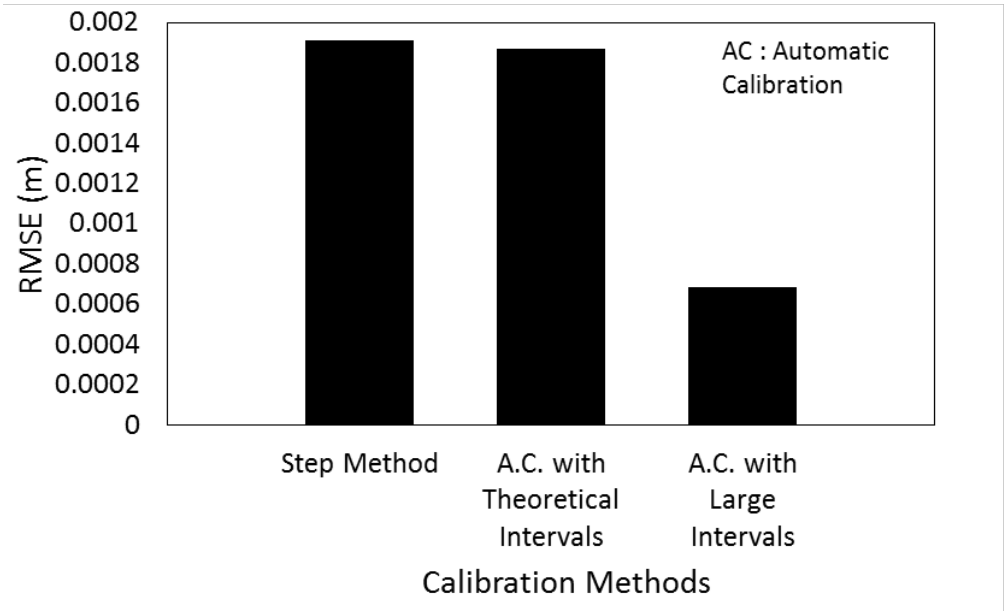

598

599 Fig. 14

600